Temporal Simultons in Optical Parametric Oscillators

Marc Jankowski,[1,*] Alireza Marandi,[1,†] C. R. Phillips,[2] Ryan Hamerly,[1] Kirk A. Ingold,[3] Robert L. Byer,[1] and M. M. Fejer[1]

[1]*Edward L. Ginzton Laboratory, Stanford University, Stanford, California 94305, USA*
[2]*Department of Physics, Institute of Quantum Electronics, ETH Zurich, Zurich 8093, Switzerland*
[3]*Photonics Research Center, U.S. Military Academy, West Point, New York 10996, USA*

(Received 26 July 2017; published 1 February 2018)

We report the first demonstration of a regime of operation in optical parametric oscillators (OPOs), in which the formation of temporal simultons produces stable femtosecond half-harmonic pulses. Simultons are simultaneous bright-dark solitons of a signal field at frequency ω and the pump field at 2ω, which form in a quadratic nonlinear medium. The formation of simultons in an OPO is due to the interplay of nonlinear pulse acceleration with the timing mismatch between the pump repetition period and the cold-cavity round-trip time and is evidenced by sech^2 spectra with broad instantaneous bandwidths when the resonator is detuned to a slightly longer round-trip time than the pump repetition period. We provide a theoretical description of an OPO operating in a regime dominated by these dynamics, observe the distinct features of simulton formation in an experiment, and verify our results with numerical simulations. These results represent a new regime of operation in nonlinear resonators, which can lead to efficient and scalable sources of few-cycle frequency combs at arbitrary wavelengths.

DOI: 10.1103/PhysRevLett.120.053904

Introduction.—The temporal modes that arise from cavity nonlinear dynamics have attracted intense interest due to both their diversity of operating regimes and their applications. Recent work has focused on resonators with cubic nonlinearities that form dissipative solitons from a balance between intracavity dispersion and self-phase modulation [1–3]. These systems have successfully generated few-cycle pulses and phase-stabilized frequency combs in the range from 400 nm to 3.5 μm [4–6] and have been employed in optical clocks [7], spectroscopy [8], telecommunications [9], and attoscience [10]. While considerable effort is being invested to extend these sources to other wavelength ranges [11], such operation requires overcoming the challenges associated with developing broadband laser gain media and high finesse resonators at new wavelengths.

Nonlinear resonators based on quadratic nonlinearities offer a compelling new direction for the field. In contrast with cubic nonlinearities, the $\chi^{(2)}$ associated with quadratic nonlinearities may be patterned to quasiphasematch a rich variety of multiwave interactions. $\chi^{(2)}$ materials are well developed and frequently used to produce pulses at otherwise inaccessible wavelengths, but many of the regimes of operation in these systems remain relatively unexplored. One promising system is the synchronously pumped degenerate optical parametric oscillator (OPO), in which a $\chi^{(2)}$ resonator pumped at 2ω generates a resonant half-harmonic at ω. While many pulse formation mechanisms have been proposed in continuous-wave-pumped degenerate OPOs [12–15], to date these systems have not yet achieved mode-locked femtosecond pulses by using such dynamics [16,17]. Conversely, synchronously pumped degenerate OPOs have been used successfully to generate half-harmonic combs, but their pulse formation mechanisms are less understood. Key results include the demonstration of instantaneous octave-spanning spectra [18], few-cycle pulses [19], intrinsic phase and frequency locking [20] (which translates the coherence properties of the pump source onto the half-harmonic signal), and conversion efficiencies as high as 64% [21,22]. Recent work suggests a number of competing pulse formation mechanisms exist in such OPOs [22].

In this Letter, we introduce and demonstrate a regime of operation in a near-synchronously pumped degenerate OPO in which stable half-harmonic pulses are formed by temporal simultons. This Letter will proceed in three parts. (i) We develop a reduced model of simulton formation and explain the characteristics of simultons in the context of OPO operation. (ii) We present experimental results and identify signatures of simulton formation. (iii) Numerical simulations are used to better understand the underlying dynamics and are shown to capture the behavior exhibited by the OPO. Based on the agreement between these three parts, we are able to connect the proposed intracavity simulton dynamics to the observed behavior of the OPO.

Theory.—Temporal simultons are simultaneous bright-dark solitons of the signal at ω and the pump at 2ω, which occur in a degenerate traveling wave optical parametric amplifier (OPA) due to group velocity mismatch and gain saturation [23,24]. The coupled wave equations for phase-matched OPA are

$$\partial_z A_\omega(z,t) = \kappa A_{2\omega} A_\omega^* + \hat{D}_\omega A_\omega, \tag{1a}$$

$$\partial_z A_{2\omega}(z,t) = -\Delta\beta' \partial_t A_{2\omega} - \kappa A_\omega^2 + \hat{D}_{2\omega} A_{2\omega}, \tag{1b}$$

where we have shifted the time coordinate to be comoving with the group velocity of the signal wave and include a $\pi/2$ phase in the pump envelope to make the equations of motion and their solutions real, assuming negligible higher order dispersion. A_ω is the field envelope, normalized such that $|A_\omega|^2$ is the instantaneous power of the ω wave, and $\Delta\beta' = v_{g,2\omega}^{-1} - v_{g,\omega}^{-1}$ is the group velocity mismatch. $\kappa = \sqrt{2\eta_0}\omega d_{\text{eff}}/(w_0 n_\omega \sqrt{\pi n_{2\omega}} c)$ is the nonlinear coupling, where d_{eff} is the effective nonlinear coefficient and η_0 is the impedance of free space. Here we have assumed the pump and the signal are confocal near-field Gaussian beams, with a $1/e^2$ beam radius of w_0 for the signal. The dispersion operator $\hat{D}_\omega = \sum_{j=2}^{\infty}[(-i)^{j+1}\beta_\omega^{(j)}/j!]\partial_t^j$ contains contributions from higher dispersion orders, where $\beta_\omega^{(j)}$ represents the jth derivative of propagation constant β at frequency ω. When $\hat{D}_\omega$ and $\hat{D}_{2\omega}$ are negligible, given the bandwidth of the pulses and the length of the nonlinear medium, the simulton solution of a traveling wave OPA is given by [23,24]

$$A_\omega(z,t) = \frac{a}{\sqrt{2\tau}}\operatorname{sech}\left(\frac{t-T}{\tau}\right), \tag{2a}$$

$$A_{2\omega}(z,t) = -E_{2\omega}\tanh\left(\frac{t-T}{\tau}\right), \tag{2b}$$

where $a^2 = 2(\Delta\beta' + \gamma_0\tau)\gamma_0/\kappa^2$ is the signal pulse energy, τ is the pulse width, $T = -\gamma_0\tau z$ represents a shift in the signal pulse relative to linear propagation due to gain saturation, and $\gamma_0 = \kappa E_{2\omega}$ is the small-signal gain coefficient. Simultons occur when the leading edge of a bright sech^2 signal pulse depletes a quasicontinuous wave pump, and the trailing edge converts back to the pump frequency through second harmonic generation (SHG) with a π phase relative to the undepleted pump [Fig. 1(a)]. The pump forms a $\tanh^2$ dark soliton coupled to the bright sech^2 signal pulse, and the pair copropagate with an intensity dependent velocity that exceeds that of either wave, $v_{g,\text{sim}}^{-1} = v_{g,\omega}^{-1} - \gamma_0\tau$.

We generalize this solution to include gain and loss using the manifold projection method described in [22] and obtain the evolution of the parameters a, τ, and T of the sechlike signal pulse from Eq. (2a). When $\Delta\beta' z \gg \tau$, $a(z)$, $T(z)$, and $\tau(z)$ evolve as

$$\partial_z a = \gamma_0 a\left(1 - \frac{a^2}{a_{\text{sim}}^2}\right), \tag{3a}$$

$$\partial_z T = -\gamma_0\tau\frac{a^2}{a_{\text{sim}}^2}, \tag{3b}$$

$$\partial_z \tau = 0. \tag{3c}$$

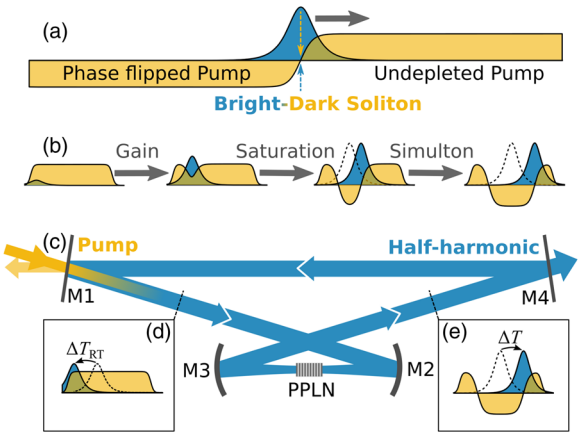

FIG. 1. (a) Field envelopes of a simulton, showing the sech-pulse signal (blue) and tanh pump (orange). (b) Evolution of pump and signal fields in an OPA from the linear to the simulton regimes. Dotted line is the evolution of the signal field undergoing linear temporal walk-off. (c) Schematic of the synchronously pumped OPO cavity. Cavity length adjustments are made by mounting $M1$ on a piezostage. (d),(e) Displacement of intracavity signal relative to a perfectly synchronous half-harmonic pulse undergoing linear propagation (dotted lines). (d) After $M1$, the signal acquires a small delay, ΔT_{RT}, relative to the incoupled pump due to the timing mismatch. (e) After optical parametric amplification, the signal acquires a nonlinear shift in group delay ΔT due to simulton formation, which compensates the timing mismatch ΔT_{RT}.

Here $a_{\text{sim}}^2 = 2\Delta\beta'\gamma_0/\kappa^2$ is the simulton energy, and we have approximated the pump as a flattop pulse, $A_{2\omega}(0,t) = \max\left(A_{2\omega}(0,t)\right)$. Equations (3a)–(3c) can be understood in two limits. When $a \ll a_{\text{sim}}$, we recover the evolution of a degenerate OPA with an undepleted pump. The signal is amplified as $a(z) = a(0)e^{\gamma_0 z}$ and propagates with a linear group velocity, i.e., $\partial_z T = 0$. When $a = a_{\text{sim}}$, we recover the simulton [Eqs. (2a) and (2b)]. In the limit of the approximations made here, the simulton solution is a stable attractor. If a sech signal pulse is seeded into a degenerate OPA such that $a > a_{\text{sim}}$, it will transfer energy to the pump through SHG until the simulton solution is reached. Equations (3a) and (3b) can be solved for the full evolution of a dissipative simulton, resulting in

$$a(z) = \frac{a(0)e^{\gamma_0 z}}{\sqrt{1 + \frac{a^2(0)}{a_{\text{sim}}^2}(e^{2\gamma_0 z} - 1)}}, \tag{4a}$$

$$\Delta T(z) = \tau\ln\left(\frac{a(0)e^{\gamma_0 z}}{a(z)}\right). \tag{4b}$$

$\Delta T(z) = T(z) - T(0)$ is the shift in group delay accumulated due to nonlinear acceleration in a single pass through the OPA crystal. A schematic of simulton formation is illustrated in Fig. 1(b), showing the evolution of the pump and signal fields in an OPA from the linear to the simulton regimes. The signal is seen to undergo linear temporal walk-off due to group velocity mismatch and extract gain

until the pump is depleted. Once depleted, the pump forms a copropagating dark soliton and the pair propagates at the simulton velocity.

Figures 1(c)–1(e) show the dynamics of a simulton OPO. On each round-trip, a new pump pulse enters the cavity through the input coupler $M1$ [Fig. 1(c)], and the signal accumulates a small group delay ΔT_{RT}, hereafter referred to as the timing mismatch, due to an offset between the pump repetition period and the cold-cavity round-trip time [Fig. 1(d)]. After passing through the OPA crystal, labeled PPLN (periodically poled lithium niobate), the signal is amplified and accumulates a simulton group advance ΔT [Fig. 1(e)]. The signal is partially outcoupled through $M4$, with a fraction R of the power returning to $M1$. Simulton formation in an OPO is a double balance of energy and timing in which the gain extracted over an OPA crystal of length L balances the cavity loss $a^2(0) = Ra^2(L)$ and the simulton acceleration balances the timing mismatch $\Delta T(L) = \Delta T_{\mathrm{RT}}$. When the timing condition is satisfied, the signal becomes synchronous with the pump and forms a half-harmonic pulse that inherits both its carrier-envelope offset frequency and comb spacing from the pump. The equations for steady state, with Eqs. (4a) and (4b), determine the simulton pulse width

$$\tau = \frac{2\Delta T_{\mathrm{RT}}}{2\gamma_0 L + \ln(R)}. \tag{5a}$$

The pulse width of a simulton OPO is seen to shrink with increasing pump power, in contrast to the conventional $\tau \propto \sqrt{P}$ "box-pulse" scaling developed in [22]. For positive detunings ($\Delta T_{\mathrm{RT}} > 0$), the simulton group advance allows for the formation of half-harmonic pulses that are synchronous with the pump at multiple cavity lengths. Negatively detuned ($\Delta T_{\mathrm{RT}} < 0$) simultons cannot form when $\Delta\beta' > 0$, since pump depletion only provides a group advance for the signal pulse. Instead, the OPO operates in a nondegenerate regime analyzed in [22]. The timing mismatch is thus a critical design parameter that determines both the mode of operation and the bandwidth of the OPO.

Experimental results.—We study the behavior of an OPO as the timing mismatch is varied around perfect synchronization with the pump. The OPO cavity (see Supplemental Material [25]) consists of a bow tie resonator with a tunable round-trip delay of ~4 ns [Fig. 1(c)] and a large output coupling of $(1 - R) = 65\%$ for the signal. OPA occurs in a 1-mm-long Brewster-cut MgO-doped PPLN crystal placed at the focus between $M2$ and $M3$. The PPLN crystal has a poling period of 31.8 μm to phase-match degenerate OPA of a signal at 2090 nm, and is pumped by 70 fs pulses at 250 MHz produced by a 1045-nm mode-locked Yb-fiber laser (Menlo Systems Orange A) with an average power of up to 950 mW. The OPO is only resonant for the signal and oscillates around cavity lengths where the signal acquires a phase shift of zero or π relative to the pump on each round-trip, leading to a discrete set of resonances whose behavior depends strongly on the timing mismatch.

We first consider the resonance at which the OPO cavity is most nearly synchronized to the pump repetition rate, labeled peak 0 in Fig. 2(a). The synchronous peak has the lowest threshold (175 mW), a slope efficiency of 158%, and a peak conversion efficiency of 46%. Moreover, it exhibits a sech^2 spectrum, which loses bandwidth with increasing power [Figs. 2(b) and 2(c)], in accordance with the conventional box-pulse scaling [22]. As the cavity is

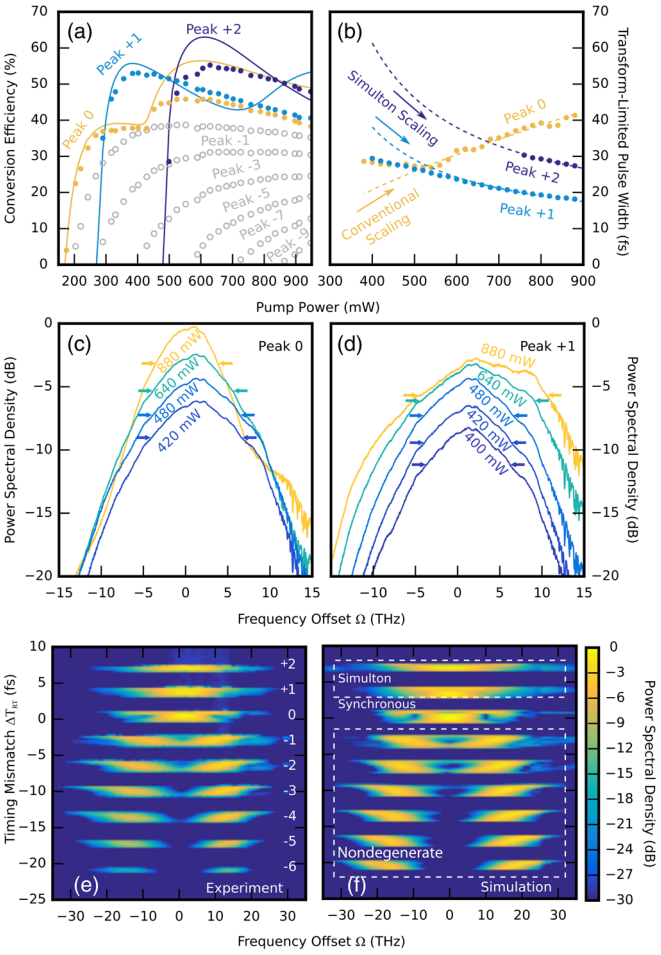

FIG. 2. (a) Measured conversion efficiency for each resonance, with the resonances enumerated relative to perfect synchronization. Positive "peak" numbers correspond to a long cavity. Solid lines represent numerical simulations of peak 0, +1, and +2, and empty gray circles denote nondegenerate operation. (b) The scaling with pump power of the transform limited pulse width (3 dB) for peaks 0–2, computed from spectra such as those shown in (c) and (d). For large powers, peak 0 shows an increase in pulse width in accordance with [22], while peaks +1 and +2 show a monotonic decrease in pulse width, which agrees well with Eq. (5a). (c),(d) (Color lines) Spectra recorded as a function of pump power for peak 0 and +1, respectively. Each curve is labeled with the corresponding pump power used in the experiment, with arrows denoting the 3 dB bandwidth. (e) Measured signal spectrum as a function of timing mismatch for a 550 mW pump, with the associated peak numbers. (f) Simulated signal spectrum in decibels relative to the maximum value, as a function of timing mismatch, with the three regimes we have identified indicated.

positively detuned ($\Delta T_{\mathrm{RT}} > 0$), two more resonances are found, labeled peak $+1$ and $+2$ in Fig. 2(a). These "long cavity" resonances have irregularly spaced thresholds as ΔT_{RT} becomes increasingly positive and have measured slope efficiencies as high as 570%, with peak efficiencies of 55%. Peaks $+1$ and $+2$ exhibit sech^2 spectra that monotonically increase in bandwidth as the pump power is increased [Figs. 2(b) and 2(d)] in accordance with the simulton scaling [Eq. (5a)]. The spectra deviate from the exponential tails of a sech^2 spectrum beyond ± 10 THz due to atmospheric absorption around 1850 nm. Peak $+1$ achieves a 3 dB bandwidth as high as 240 nm, which can support pulses as short as 19 fs. When the cavity is negatively detuned ($\Delta T_{\mathrm{RT}} < 0$), the OPO transitions to nondegenerate operation and the spectra split into a distinguishable signal and idler [Fig. 2(e)]. The peaks in the nondegenerate regime exhibit thresholds that increase uniformly as ΔT_{RT} becomes increasingly negative, slope efficiencies less than 40%, and conversion efficiencies less than 40% [Fig. 2(a)]. We therefore identify three regimes of operation associated with the timing mismatch: synchronous ($\Delta T_{\mathrm{RT}} = 0$), nondegenerate ($\Delta T_{\mathrm{RT}} < 0$), and simulton ($\Delta T_{\mathrm{RT}} > 0$).

Simulation.—To better understand the dynamics that determine the three regimes of operation observed in the experiment and verify that the positively detuned resonances correspond to simulton operation, we study the OPO using numerical methods. The OPO is modeled as an OPA followed by a linear feedback loop. On each round-trip, we solve Eqs. (1a) and (1b) using split-step Fourier methods, including all dispersion orders computed from the dispersion relations given in [27]. We model the feedback loop as a linear filter for the signal

$$A_{\omega}^{(n+1)}(0,t) = \mathcal{F}^{-1}\{\sqrt{R(\Omega)}e^{-i\phi(\Omega)}\mathcal{F}\{A_{\omega}^{(n)}(L,t)\}\}.$$

The phase $\phi(\Omega)$ is measured relative to a half-harmonic signal, which is perfectly synchronous with the pump

$$\phi(\Omega) = \phi_0 + \pi l + \Delta T_{\mathrm{RT}}\Omega + \Delta\phi(\Omega),$$

where ϕ_0 represents an offset between the cavity resonances and the cavity length, which synchronizes the pump and signal, $\Delta\phi(\Omega)$ represents the quadratic and higher order dispersion of the cavity mirrors, and $l = c\Delta T_{\mathrm{RT}}/\lambda_{2\omega}$ parametrizes the peak number as the cavity length is varied from perfect synchronization, with resonances centered on cavity lengths such that $l \in \mathbb{Z}$. Further details of $R(\Omega)$ and $\Delta\phi(\Omega)$ are discussed in the Supplemental Material [25].

The solid lines in Fig. 2(a) show the simulated conversion efficiency of the resonances in the synchronous and simulton regimes and are shown to be in good agreement with the experimental thresholds and slope efficiencies. Deviations that occur at higher powers are likely due to radial variations in pump depletion not included in the simulation. A simulation of the spectrum as a function of timing mismatch with parameters corresponding to the experiment is shown in Fig. 2(f), with the three regimes of operation indicated by the dashed boxes. The simulations show excellent agreement with the experimental data [Fig. 2(e)] in all three operating regimes. In the case of $\Delta T_{\mathrm{RT}} > 0$, stable femtosecond half-harmonic pulses are generated through the formation of simultons.

Having shown agreement between the numerical model and experiment, we now use the model to better understand the femtosecond pulse formation dynamics in the OPO. The evolution of the signal pulse is shown in Figs. 3(a)–3(c) for each of the three regimes of operation. Each round-trip is recorded at the output of the OPA and normalized to its peak amplitude to visualize the pulse motion. The dotted white lines show the expected trajectory of a linearly propagating half-harmonic signal pulse, which acquires a delay ΔT_{RT} on every round-trip. In these figures, the time coordinates have been shifted such that a signal peaked at $t = 0$ corresponds to a pulse walking symmetrically from the tail of the pump at $\Delta\beta' L/2$ to the leading edge of the pump $-\Delta\beta' L/2$. For a negatively detuned peak [Fig. 2(a)], the pulse envelope shows a 10 THz modulation in time (vertical fringes), resulting from interference of a signal and idler split from degeneracy by ± 10 THz. The interference fringes are seen to shift on each round-trip, corresponding to a ± 10 MHz offset of the signal and idler carrier-envelope offset (CEO) frequency f_{CEO} from

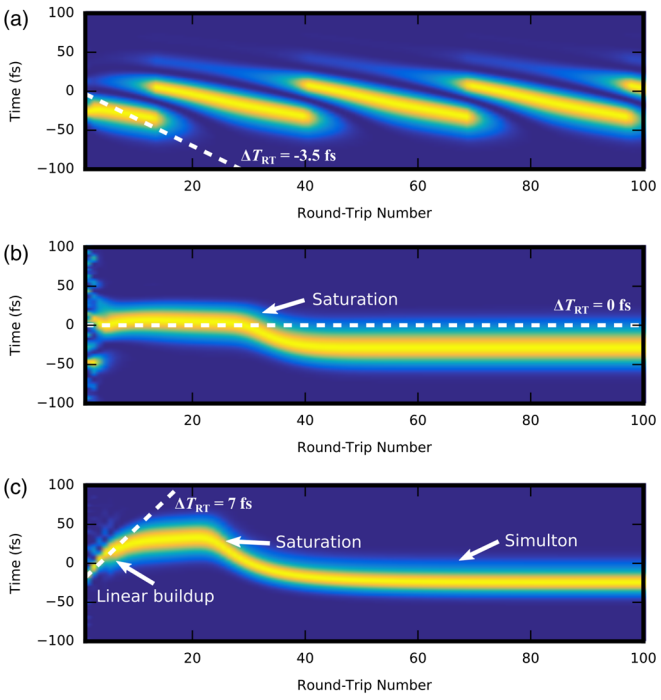

FIG. 3. (a) Simulated evolution of the intracavity pulse intensity over many round-trips for $\Delta T_{\mathrm{RT}} = -3.5$ fs showing the interference of a distinct signal and idler. The dotted line denotes the trajectory of a linearly propagating half-harmonic signal pulse. (b) Pulse evolution for $\Delta T_{\mathrm{RT}} = 0$ fs showing the formation of a half-harmonic pulse synchronized to the pump repetition rate. (c) Simulated pulse evolution for $\Delta T_{\mathrm{RT}} = 7$ fs showing the formation of a half-harmonic pulse which, upon depleting the pump, is able to accelerate forward in time and synchronize to the pump repetition rate.

that of a half-harmonic signal (horizontal fringes). When the cavity length is tuned into synchronization [Fig. 2(b)], the signal builds up without any motion relative to the pump until the pump saturates, shifting the signal forward in time until a new steady state is found on the leading edge of the pump. The evolution for a positively detuned cavity is shown in Fig. 2(c). The signal initially tracks the trajectory of a linearly propagating pulse, shifting toward the tail of the pump. Once the signal is intense enough to deplete the pump, it accelerates, becoming faster than would be possible under linear propagation and thereby reaches a steady state, synchronous with the pump repetition rate.

The surprising behavior exhibited by the long cavity resonances, namely, a nonlinear acceleration of the signal pulses, indicates that the OPO dynamics in this regime correspond to simulton formation. Furthermore, the full numerical model facilitates an intuitive picture of the behavior of the simulton peaks. The large thresholds and slope efficiencies of the simulton peaks are due to the pulse width of the pump. When $a \ll a_{\mathrm{sim}}$, the signal pulse will accumulate many successive group delays due to the timing mismatch and experience a decrease in gain due to a reduction in the temporal overlap with the pump. Since simulton operation requires the signal to be bright enough to deplete the pump, the threshold then corresponds to the condition that the signal builds up from quantum noise to the simulton energy before the temporal walk-off reduces the gain seen by the signal pulse below the cavity loss. Once this condition is satisfied, the signal accelerates back into the pump and depletes it, leading to large slope efficiencies.

Conclusion.—We have introduced a new pulse formation mechanism based on temporal simultons in resonators with a quadratic nonlinearity. Temporal simultons form due to a competition between timing mismatch and nonlinear pulse acceleration and exhibit favorable scaling laws for the formation of few-cycle pulses at arbitrary wavelengths. We have provided experimental evidence of an OPO operating in the simulton regime and confirm that such an OPO can be used to efficiently generate sech^2 spectra with large instantaneous bandwidths in agreement with theory. Our results indicate that design rules for simulton OPOs are in sharp contrast with those of conventional OPOs, and such design rules will be the subject of future publications.

The authors would like to acknowledge support from DARPA DODOS Grant No. 2014003913-03, NSF Grant No. ECCS-1609688, and NSF-BSF Grant No. PHY-1535711.

*marcjank@stanford.edu
†marandi@stanford.edu

[1] H. A. Haus, IEEE J. Sel. Top. Quantum Electron. **6**, 1173 (2000).
[2] P. Grelu and N. Akhmediev, Nat. Photonics **6**, 84 (2012).
[3] T. Herr, V. Brasch, J. D. Jost, C. Y. Wang, N. M. Kondratiev, M. L. Gorodetsky, and T. J. Kippenberg, Nat. Photonics **8**, 145 (2014).
[4] V. Brasch, M. Geiselmann, T. Herr, G. Lihachev, M. H. P. Pfeiffer, M. L. Gorodetsky, and T. J. Kippenberg, Science **351**, 357 (2016).
[5] A. G. Griffith, R. K. W. Lau, J. Cardenas, Y. Okawachi, A. Mohanty, R. Fain, Y. H. D. Lee, M. Yu, C. T. Phare, C. B. Poitras, A. L. Gaeta, and M. Lipson, Nat. Commun. **6**, 6299 (2015).
[6] B. Bernhardt, E. Sorokin, P. Jacquet, R. Thon, T. Becker, I. T. Sorokina, N. Picqu, and T. W. Hansch, Appl. Phys. B **100**, 3 (2010).
[7] S. A. Diddams, L. Hollberg, L. S. Ma, and L. Robertsson, Opt. Lett. **27**, 58 (2002).
[8] I. Coddington, N. Newbury, and W. Swann, Optica **3**, 414 (2016).
[9] P. Marin, J. N. Kemal, M Karpov, A Kordts, J Pfiele, M. H. P. Pfeiffer, P. Trocha, S. Wolf, V. Brasch, M. H. Anderson, R. Rosenberger, K. Vijayan, W. Freude, T. J. Kippenberg, and C. Koos, Nature (London) **546**, 274 (2017).
[10] M. Hentschel, R. Kienberger, Ch. Spielmann, G. A. Reider, N. Milosevic, T. Brabec, P. Corkum, U. Heinzmann, M. Drescher, and F. Krausz, Nature (London) **414**, 509 (2001).
[11] A. Schliesser, N. Picque, and T. W. Hansch, Nat. Photonics **6**, 440 (2012).
[12] S. Longhi, Opt. Lett. **20**, 695 (1995).
[13] L. A. Lugiato, C. Oldano, C. Fabre, E. Giacobino, and R. J. Horowicz, Nuovo Cimento Soc. Ital. Fis. **10D**, 959 (1988).
[14] T. Hansson, F. Leo, M. J. Erkintalo, J. Anthony, S. Coen, I. Ricciardi, M. De Rosa, and S. Wabnitz, J. Opt Soc. Am. B **33**, 1207 (2016).
[15] F. Leo, T. Hansson, I. Ricciardi, M. De Rosa, S. Coen, S. Wabnitz, and M. Erkintalo, Phys. Rev. Lett. **116**, 033901 (2016).
[16] V. Ulvila, C. R. Phillips, L. Halonen, and M. Vainio, Opt. Lett. **38**, 4281 (2013).
[17] V. Ulvila, C. R. Phillips, L. Halonen, and M. Vainio, Opt. Express **22**, 10535 (2014).
[18] Q. Ru, N Lee, X Chen, K Zhong, G Tsoy, M Mirov, S Vasilyev, S. B. Mirov, and K. L. Vodopyanov, Optica **4**, 617 (2017).
[19] R. A. McCracken and D. T. Reid, Opt. Lett. **40**, 4102 (2015).
[20] A. Marandi, N. C. Leindecker, V. Pervak, R. L. Byer, and K. L. Vodopyanov, Opt. Express **20**, 7255 (2012).
[21] A. Marandi, K. A. Ingold, M. Jankowski, and R. L. Byer, Optica **3**, 324 (2016).
[22] R. Hamerly, A. Marandi, M. Jankowski, M. M. Fejer, Y. Yamamoto, and H. Mabuchi, Phys. Rev. A **94**, 063809 (2016).
[23] S. A. Akhmanov, A. Chirkin, K. Drabovich, A. Kovrigin, R. Khokhlov, and A. Sukhorukov, IEEE J. Quantum Electron. **4**, 598 (1968).
[24] S. Trillo, Opt. Lett. **21**, 1111 (1996).
[25] See Supplemental Material at http://link.aps.org/supplemental/10.1103/PhysRevLett.120.053904 for a discussion of the modeling and design of the OPO cavity, which includes Ref. [26].
[26] A. La Porta and R. E. Slusher, Phys. Rev. A **44**, 2013 (1991).
[27] O. Gayer, Z. Sacks, E. Galun, and A. Arie, Appl. Phys. B **91**, 343 (2008).